Kobe University Repository : Kernel

PDF issue: 2026-11-19

Effective oil-in-water emulsion separation by self-cleaning superoleophobic hydrogel membrane composite with hierarchical structure

Kwon, Hyun Woong ; Gonzales, Ralph Rolly ; Zhang, Pengfei ; Li, Bowen ; Im, Kwang Seop ; Park, Jun Ho ; Lee, Tae Kyung ; Matsuyama, Hideto ;…

(Citation)
npj Clean Water,8(1):37

(Issue Date)
2025-05-10

(Resource Type)
journal article

(Version)
Version of Record

(Rights)
© The Author(s) 2025.
This article is licensed under a Creative Commons Attribution-NonCommercial-NoDerivatives 4.0 International License, which permits any non-commercial use, sharing, distribution and reproduction in any medium or format, as long as you give…

(URL)
https://hdl.handle.net/20.500.14094/0100495868

KOBE UNIVERSITY

npj | clean water

Article

Published in partnership with King Fahd University of Petroleum & Minerals

https://doi.org/10.1038/s41545-025-00468-0

Effective oil-in-water emulsion separation by self-cleaning superoleophobic hydrogel membrane composite with hierarchical structure

Check for updates

Hyun Woong Kwon[1,2,5], Ralph Rolly Gonzales[2,3,5], Pengfei Zhang[2], Bowen Li[2,4], Kwang Seop Im[1], Jun Ho Park[1], Tae Kyung Lee[1], Hideto Matsuyama[2,4] ✉ & Sang Yong Nam[1] ✉

Hollow fiber membranes were fabricated using polyvinylidene fluoride (PVDF) via the thermally induced phase separation method for oil-water separation. By introducing glycerol triacetate (GTA) or propylene carbonate as an extruded solvent, membrane porosity and pore size were controlled, significantly enhancing water permeance. The highest porosity and permeance were achieved with GTA as the co-extruded solvent. To further improve separation performance, a polyvinyl alcohol (PVA) coating was applied, forming a superhydrophilic and superoleophobic membrane composite. The coated membranes exhibited complete water absorption (0° contact angle) while repelling oil, preventing droplet adhesion. Antifouling performance was significantly improved, with flux recovery ratios exceeding 90% compared to 2–26% for uncoated membranes. The best-performing membrane achieved a high oil-in-water emulsion permeance of 3551 LMH/bar and 99.2% soybean oil removal efficiency. These findings demonstrate the potential of superhydrophilic and superoleophobic membranes with controlled porosity for efficient oil-water separation.

The continuous discharge of oily wastewater from industrial activities, household sources, and transportation poses a significant threat to environmental sustainability and public health if not properly managed[1]. Oily wastewater contains hazardous organic compounds that can cause severe water pollution, disrupt aquatic ecosystems, and pose risks to human health. Traditional treatment methods such as electrocoagulation, adsorption, and chemical separation have been widely used but often suffer from high operational costs, secondary pollution, and inefficient separation of stable oil-in-water emulsions[2–4]. In contrast, membrane filtration has emerged as a promising and efficient solution due to its ability to achieve high oil removal efficiency, operational simplicity, and cost-effectiveness compared to conventional methods[5].

Microfiltration and ultrafiltration membranes are commonly used to separate oil droplets from water. However, these membranes often experience severe fouling, particularly due to oil adhesion, which compromises long-term performance and necessitates frequent cleaning or replacement. Membrane fouling occurs because the hydrophobic nature of many conventional membranes allows oil droplets to accumulate on the surface and within the pores, ultimately reducing filtration efficiency. To address these challenges, developing membranes with superior anti-oil-fouling properties is essential for improving oil-in-water emulsion separation. Researchers have focused on modifying membrane surfaces to achieve superhydrophilicity and underwater superoleophobicity, which prevent oil adhesion and significantly reduce fouling[6].

Membrane modification strategies such as zwitterionic coatings, nano-sized particle incorporation, and electroconductive coatings have been widely explored to enhance membrane separation performance. Zwitterionic coatings improve antifouling properties by creating a hydration layer that resists the adhesion of contaminants[7–9]. The incorporation of nano-sized particles, such as graphene oxide[10,11], metal organic framework[12,13], covalent organic framework[14,15], or MXene[16,17], enhances mechanical strength, wetting properties, and selective permeability. Electroconductive coatings enable responsive membranes with tunable separation properties under an external stimulus[18,19]. While these methods are effective, they often

[1]Department of Materials Engineering and Convergence Technology, Engineering Research Institute, Gyeongsang National University, Jinju, South Korea. [2]Research Center for Membrane and Film Technology, Kobe University, Nada, Kobe, Japan. [3]Scion, Private Bag 3020, 3046 Rotorua, New Zealand. [4]Department of Chemical Science and Engineering, Kobe University, Nada, Kobe, Japan. [5]These authors contributed equally: Hyun Woong Kwon, Ralph Rolly Gonzales. ✉e-mail: matuyama@kobe-u.ac.jp; walden@gnu.ac.kr

involve complex fabrication processes, the use of specialised chemicals, and sophisticated equipment, making large-scale implementation challenging.

Like zwitterionic compounds, hydrogel-based materials have gained considerable attention due to their strong hydrophilicity and ability to form hydration layers that effectively repel oil and other contaminants[20,21]. Among these, polyvinyl alcohol (PVA) is particularly promising due to its excellent water retention capacity, mechanical flexibility, and ability to create surfaces with ultra-low oil adhesion[22–24]. Incorporating PVA onto membrane surfaces can enhance water permeability while simultaneously reducing oil fouling. However, applying hydrogel coatings onto porous membranes presents challenges, including ensuring strong adhesion between the hydrogel and membrane, maintaining long-term stability, and preserving optimal water permeation properties. Addressing these challenges requires careful selection of membrane substrates and optimization of hydrogel deposition techniques to ensure uniform coating distribution and long-term performance.

In this study, we developed a highly porous polyvinylidene fluoride (PVDF) hollow fiber membrane with a unique hierarchical spherulitic outer structure using a triple-orifice spinneret in the thermally induced phase separation (TIPS) process[25,26]. This simple yet effective approach enhances separation performance solely through the regulation of the membrane porosity. The resulting membrane structure is both porous and mechanically robust, making it an ideal substrate for hydrogel coating. A PVA hydrogel layer was subsequently deposited and crosslinked onto the outer surface of the PVDF membrane, creating a hydrogel membrane composite with significantly improved underwater oleophobicity[27]. The enhanced oleophobicity of the composite membrane prevents oil droplet adhesion, minimizing fouling and improving the separation efficiency of oil-in-water emulsions.

The greatest challenge in developing membranes with specialized wetting properties is integrating the material's intrinsic properties with the microstructural design[28]. Thus, the main objective of this work was to develop high-performance hollow fiber membranes for efficient oil-water separation by regulating their porous structure and surface properties. Instead of relying on complex chemical modifications, this study focuses on controlling pore size and porosity through solvent co-extrusion during the TIPS process. Additionally, by applying a PVA coating, the membranes were transformed into superhydrophilic and superoleophobic composites, enhancing water permeance, antifouling properties, and oil rejection. By optimising the membrane fabrication process, this work aims to achieve a simple yet effective strategy for improving separation performance, making the membranes more practical for large-scale applications in oil-water treatment.

This work represents the first reported approach that combines solvent extrusion-based membrane fabrication with hydrogel surface modification to synergistically regulate membrane hydrophilicity and oleophobicity. Membranes with hierarchical porous structures have traditionally been employed in membrane distillation due to their intrinsic hydrophobic or omniphobic properties, which help in preventing liquid penetration while allowing vapor transport. These properties are essential for maintaining separation efficiency and minimising membrane wetting during the distillation process. However, in this study, a novel approach is introduced by coating PVA onto PVDF membranes prepared via solvent co-extrusion during TIPS. This modification results in the transformation of the membrane's surface characteristics, yielding a superhydrophilic and superoleophobic membrane while retaining the hierarchical porosity. By leveraging both membrane structural design and advanced surface coating techniques, our strategy provides an innovative and practical solution for addressing the challenges associated with oily wastewater treatment. The PVA coating not only enhances water affinity but also effectively repels oils, offering potential advantages in applications requiring selective wettability, improved antifouling properties, and enhanced separation performance. The findings from this study pave the way for the development of high-performance membranes with enhanced anti-fouling properties, offering a sustainable and efficient method for industrial wastewater purification, oil spill remediation, and petrochemical wastewater management.

Results

Membrane characterization

The polyvinyl alcohol hydrogel modification was achieved through dip coating and crosslinking, as confirmed by membrane characterization. Scanning electron microscopy analysis (Fig. 1a-b) revealed distinct surface and cross-sectional morphologies for polyvinylidene membranes prepared with different extruded solvents. As shown in Fig. 1a, surface morphology varied depending on the presence and type of extruded solvent. The standard PVDF membrane, prepared without an extruded solvent, exhibited a dense surface due to rapid diluent evaporation during the air gap passage, which led to faster phase separation and a higher PVDF concentration on the external surface[25]. In contrast, membranes prepared with GTA and PC as extruded solvents showed numerous microscale surface pores. This was because diluent evaporation was prevented, and the polymer did not come into direct contact with cooling water, reducing the cooling rate and increasing pore size[29]. Despite these differences in surface morphology, all membranes—with and without an extruded solvent—exhibited a bulk cross-sectional morphology due to strong interactions between PVDF and the diluent, GTA, leading to typical solid-liquid phase separation[30–33]. The cross-sectional images (Fig. 1b.2, b.4., and b.6.) of the modified membranes confirm the successful deposition of the PVA hydration layer, which increased the thickness of the outer skin layer. The thickness of the PVA coating was measured from the cross-sectional images of the PVA-modified membranes (Figure. S1). All PVA coatings were within 3 to 5 μm thickness, with the PVA coating on the PVDF membrane prepared without solvent co-extrusion having the highest thickness (4.85 μm) while the coating thicknesses atop the PVDF membranes prepared with GTA and PC extrusion were lower (3.63 μm and 3.36 μm for M-PVDF/GTA and M-PVDF/PC, respectively). The difference in the PVA coating thickness can be attributed to the surface structure of the PVDF membranes, with the PVA coating adhering on the spherulitic hierarchical surface structure of the PVDF membranes prepared with solvent co-extrusion. SEM imaging confirms that surface pore size control can be effectively controlled by using extruded solvents, allowing for the fabrication of porous PVDF membranes.

A liquid-liquid porometer was used to determine the pore size of the fabricated porous membranes, with the average pore size and distribution shown in Fig. 1c and Figure S2. The measurements revealed variations in pore size depending on the choice of extruded solvent and its interaction with the polymer (Figure S3)[34,35], with PVA coating reducing pore sizes. The PVDF membrane without an extruded solvent had an average pore size of 21.7 nm due to rapid phase separation, facilitated by the easy evaporation of the diluent and direct contact of the polymer solution with cooling water, resulting in a dense surface layer (as seen in the SEM images)[25]. In contrast, membranes with extruded solvents exhibited increased pore sizes, while PVA hydrogel coatings increased membrane thickness, enabling controlled porosity. The average pore sizes of membranes prepared with GTA and PC as extruded solvents were 320 μm and 286 μm, respectively. These differences in pore size can be attributed to differences in solubility parameters between the extruded solvent and PVDF, as well as between the extruded solvent and the diluent, as shown in Table S2 and illustrated in Figure S4. In general, when $|\delta t(\text{solvent}) - \delta t(\text{diluent})|$ is small and $|\delta t(\text{solvent}) - \delta t(\text{PVDF})|$ is large, stronger interactions between the diluent and extruded solvent promote the formation of a more porous structure. Using GTA, which exhibits strong interactions with PVDF, as an extruded solvent results in a larger pore size by reducing PVDF concentration at the surface during air gap passage. After PVA coating, the pore size of the M-PVDF membrane was too small (less than 13 μm) to be accurately measured, while the pore sizes of M-PVDF/GTA and M-PVDF/PC decreased to 197–114 nm due to the presence of the PVA hydrogel layer.

To confirm the success of the PVA coating and GA cross-linking, further membrane characterization was conducted. Fourier transform infrared spectroscopy (Figure S4) and X-ray photoelectron spectroscopy (Figure S5, Table S1) analyses confirmed successful hydrogel coating, with new -OH and oxygen peaks, reduced fluorine content, and enhanced hydrophilicity. Unlike the untreated porous membrane, the PVA-coated

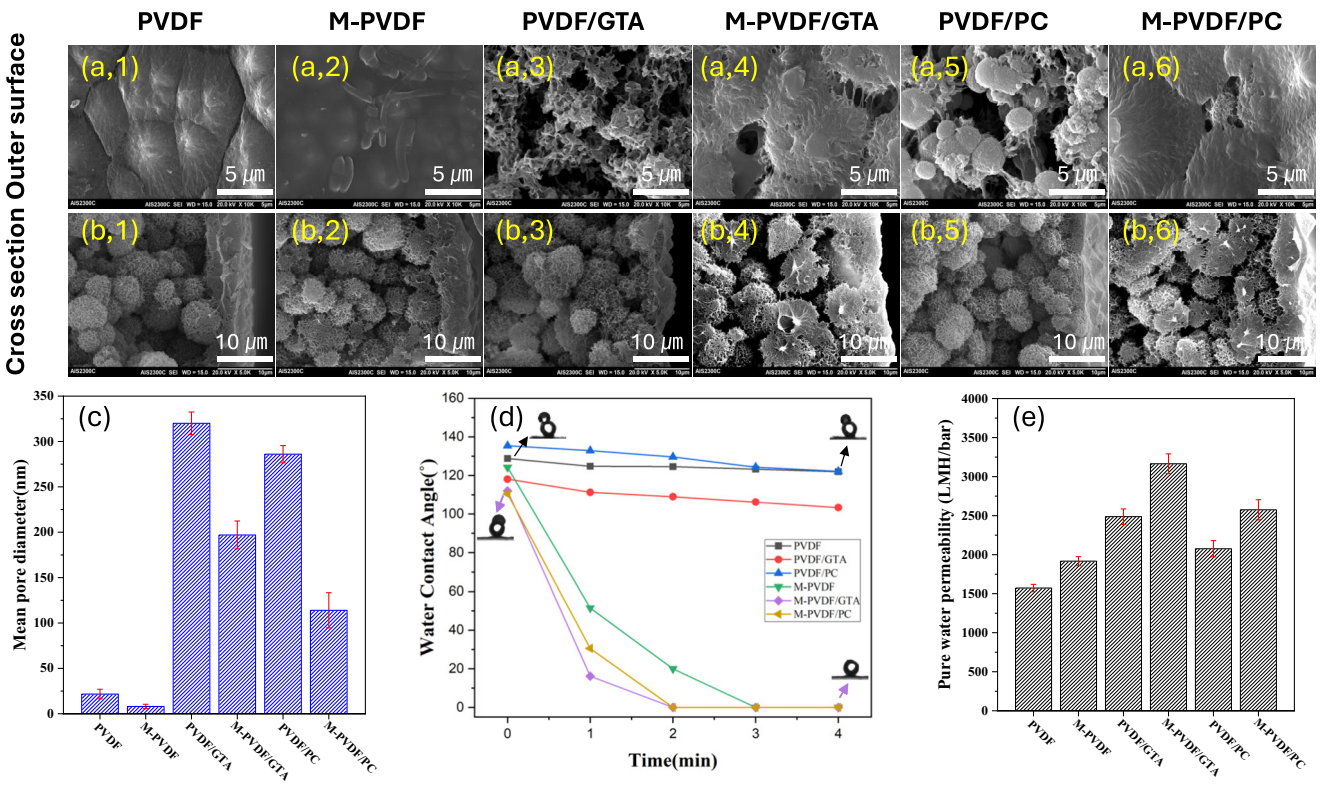


Fig. 1 | Membrane characterization results of the membranes prepared in this work. (**a**) Outer surface and (**b**) cross section morphology, (**c**) mean surface pore size, (**d**) water contact angle, and (**e**) pure water permeance.

membranes exhibited a new absorption peak between 3300 and 3400 cm^{-1}, corresponding to the broad -OH group of PVA[27]. Additionally, CH_2 peaks, indicative of GA cross-linking, were observed around 2920 to 2950 cm^{-1} [24]. These findings confirm the successful deposition of the PVA coating layer on the porous membrane surface and the formation of GA cross-links. The deconvoluted high-resolution narrow scan spectra (Figure S6) revealed the presence of alcohol groups and acetal groups in the PVA-modified membrane, differentiating these membranes from the pristine PVDF membrane, which only exhibited the presence of C-H and C-F groups[36]. Surface chemical composition analysis via XPS revealed the appearance of a new oxygen peak in all PVA-coated membranes. The elemental composition of C, F, and O for all porous membranes is listed in Table S1. Before PVA coating, the fluorine content on the membrane surface ranged from 49 to 55%. After coating, the fluorine content decreased to 32–33%, while the oxygen content, attributed to the formation of the PVA hydration layer, increased to 13.4–13.5%. These FT-IR and XPS measurements confirmed successful hydrophilic surface modification of each porous membrane.

Zeta potential measurements (Figure S7) further confirmed increased surface negative charge after PVA coating due to functional group effects. The zeta potential was measured over a pH range of 3 to 11 to compare surface charge before and after PVA coating. Before coating, the porous membranes exhibited a slightly negative charge across the entire pH range due to the inherent properties of PVDF. After PVA coating and GA crosslinking, the membranes maintained a negative charge but displayed more negative values from pH 4 to 11, attributed to functional groups like the hydroxyl groups in PVA and aldehyde groups in GA. These hydroxyl groups contributed to a stronger negative charge upon dissociation[37].

Mechanical strength tests (Table S2) demonstrated that the hydrogel coating improved tensile strength and elongation by enhancing cross-linking and crystalline structure[38]. From SEM analysis, the PVDF membrane with the densest surface layer exhibited relatively higher tensile strength and elongation compared to membranes prepared with extruded solvents. The maximum stress and elongation values for the pristine PVDF membrane were 6.6 MPa and 66.9%, respectively. The membrane prepared with GTA as the extruded solvent exhibited maximum stress and elongation values of 5.4 MPa and 40.0%, while the membrane prepared with PC had the lowest values of 2.9 MPa and 47.7%, respectively. After PVA coating, the tensile strength and elongation values increased. The M-PVDF membrane exhibited values of 7.6 MPa and 76.9%, the M-PVDF/GTA showed 6.9 MPa and 37.4%, and the M-PVDF/PC exhibited 3.1 MPa and 48.8%. These improvements are attributed to chemical cross-linking between PVA molecules via GA, which enhances the crystalline structure of the membrane and increases resistance to external forces. Uniform cross-linking improves stress distribution, resulting in enhanced tensile strength.

To evaluate hydrophilicity after modification, water contact angles (WCA) measurements were performed (Fig. 1d). Unmodified PVDF membranes exhibited high hydrophobicity, whereas the hydrogel-coated membranes exhibited complete hydrophilicity, allowing uniform water spreading due to strong hydrogen bonding and the smooth surface from the hydrogel layer. For uncoated membranes, water droplets remained on the surface for up to 4 minutes due to PVDF's inherent hydrophobicity. The initial WCA of the uncoated PVDF membrane was 124.2°, decreasing slightly to 122° after 4 minutes, confirming its intrinsic hydrophobicity. Similarly, the initial WCA values for the PVDF/GTA and PVDF/PC membranes were 118.1° and 135.4°, respectively, decreasing to 103.3° and 122.2° after 4 minutes, indicating sustained hydrophobicity. In contrast, the PVA-coated M-PVDF membrane's WCA dropped from 124.2° to 0° within 4 minutes, confirming complete hydrophilicity. Both the M-PVDF/GTA and M-PVDF/PC membranes also reached a WCA of 0 within 2 minutes, demonstrating their hydrophilic nature. This improvement is attributed to PVA's ability to form strong hydrogen bonds with water, enabling water to uniformly spread across the surface.

Oleophobicity is a crucial property for oil/water emulsion separation. Therefore, the oleophobic properties before and after PVA coating were compared using underwater oil contact angle (OCA) measurements for a variety of oils, including chloroform, soybean oil, hexane, hexadecane,

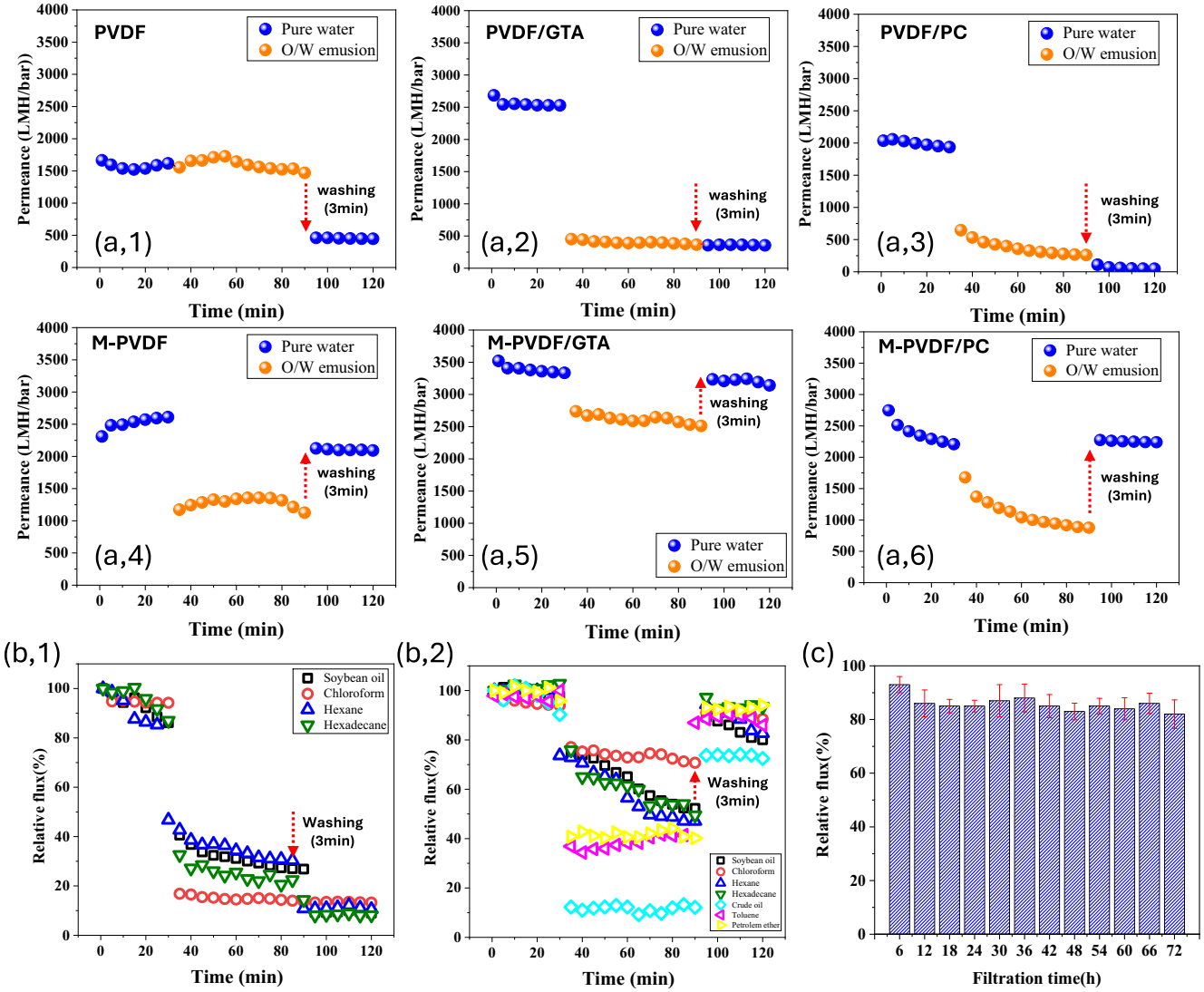


Fig. 2 | Fouling resistance evaluation of the membranes prepared in this work. **a** Pure water and soybean oil-in-water emulsion permeance of the membranes prepared in this work after one cycle of filtration tests; **b** Pure water and emulsion permeance of PVAF/GTA and M-PVDF/GTA membranes using different oil-in-water emulsions; **c** Filtration performance of the M-PVDF/GTA membrane over three days (six 12-hour cycles). Feed solution: 1 wt% soybean oil-in-water emulsion.

toluene, petroleum ether, and crude oil. As shown in Figure S8, chloroform did not adhere to the hydrophilic surface after PVA/GA coating, preventing OCA measurement. Figure S9 shows OCA measurements for hexadecane, hexane, and soybean oil before PVA/GA coating, where the high hydrophobicity of PVDF caused the oils to rapidly penetrate the surface, resulting in OCA values of 0°. In contrast, after PVA coating (Figure S10 and S11), none of the oils adhered to the hydrophilic surface, similar to the behavior observed for chloroform. This confirms the successful modification of the surface, demonstrating oleophobicity.

Pure water permeance was measured using a laboratory-scale filtration setup, with results shown in Fig. 1e. The PVDF porous membrane without extrusion exhibited a lower pure water permeance of 1573 LMH/bar compared to the membranes made with extruded solvents GTA and PC. Specifically, the PVDF/PC membrane had a permeance of 2076 LMH/bar, while the PVDF/GTA membrane had the highest value of 2487 LMH/bar. This aligns with the SEM and pore size results, where the PVDF/ GTA membrane, with the largest pore size, achieved the highest permeance, while the denser skin layer of the PVDF membrane resulted in lower permeance. After PVA coating, the pure water permeance values increased for all membranes. The M-PVDF membrane's permeance rose from 1573 LMH/bar to 1917 LMH/bar, the M-PVDF/PC membrane increased from 2076 LMH/bar to 2575 LMH/bar, and the M-PVDF/GTA membrane increased from 2487 LMH/bar to 3165 LMH/bar. This improvement is attributed to the hydrophilic nature of the hydrogel coating, which enhances water adsorption and diffusion, even with reduced pore size, as indicated by the WCA measurements.

The self-cleaning ability of the membranes was evaluated using Oil Red O dye mixed with soybean oil and chloroform. The PVDF hollow fiber membranes prepared using GTA as the extruded solvent were used. As shown in Figs. S12 and S13, the PVDF/GTA and M-PVDF/GTA membranes were immersed in water after dyed oil exposure. The uncoated PVDF/GTA membrane exhibited strong oil adhesion and penetration, preventing oil removal even with shaking. In contrast, the PVA-coated M-PVDF/GTA membrane repelled oil, allowing easy detachment upon immersion and gentle shaking, demonstrating effective self-cleaning properties.

Anti-fouling properties play a critical role in reducing membrane fouling in water treatment processes. To assess these properties, membrane permeability was compared before and after polyvinyl alcohol (PVA/GA) coating (Fig. 2a, Table S4). Coated membranes showed significant permeability recovery and higher flux recovery ratios (FRR), indicating improved resistance to fouling. Anti-fouling performance was tested using soybean

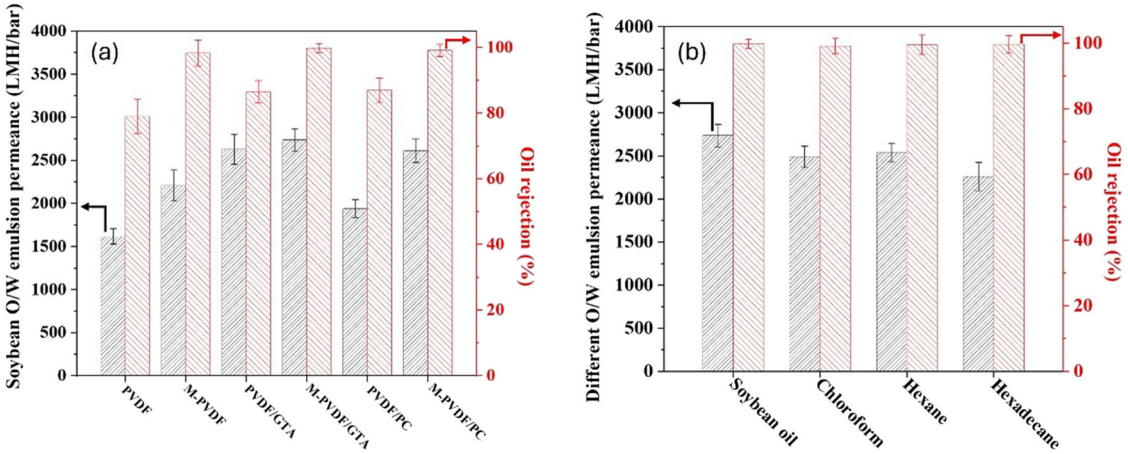


Fig. 3 | Oil-in-water emulsion separation performance of the membranes prepared in this work. a Separation performance of the membranes prepared in this work using soybean oil-in-water emulsion, and (**b**)Separation performance of M-PVAF/GTA membrane using different oil-in-water emulsions.

oil-in-water emulsions, where permeation followed a water–oil emulsion–water cycle. Uncoated membranes (PVDF, PVDF/GTA, PVDF/PC) suffered substantial permeability loss, with values dropping from 1664, 2684, and 2035 LMH/bar to 446, 355, and 47 LMH/bar, respectively. In contrast, PVA/GA-coated membranes (M-PVDF, M-PVDF/GTA, M-PVDF/PC) retained significantly higher permeability, decreasing only slightly from 2310, 3551, and 2748 LMH/bar to 2124, 3334, and 2274 LMH/bar, respectively.

FRR measurements (Table S3) confirmed this trend. Uncoated membranes exhibited poor recovery (26.8% for PVDF, 13.3% for PVDF/GTA, and 2.3% for PVDF/PC). However, after PVA/GA coating, FRR values increased dramatically to 92%, 93.9%, and 82.8%, respectively, demonstrating effective anti-fouling performance due to hydrophilic surface modification.

Further testing with chloroform, hexane, and hexadecane emulsions (Fig. 2b, Table S4) showed that the M-PVDF/GTA membrane maintained over 90% FRR for all tested oils, confirming its superior resistance to fouling.

The results shown in Fig. 2c that even in extended operation of oil-in-water emulsion filtration, the best-performing membrane (M-PVDF/GTA) exhibited stable performance, retaining over 82% of its initial flux even after three days. This stability in flux performance indicates the stability of the PVA coating and its ability to control the occurrence of fouling even after extended use.

The fouling resistance of membranes is influenced by their hydrophilicity, oleophobicity, and surface morphology before and after PVA/GA coating. Uncoated PVDF membranes have a rough, dense surface due to rapid phase separation during fabrication, leading to high hydrophobicity and a high water contact angle (WCA). After PVA/GA coating, the membrane surface becomes smoother and more uniform. The hydrophilic hydroxyl groups in PVA form strong hydrogen bonds with water molecules, allowing water to spread evenly across the surface, reducing the WCA to 0° and achieving complete hydrophilicity. This smooth, hydrophilic surface enhances water attraction and spreading.

Initially, the rough PVDF surface allows oil droplets to penetrate and adhere, resulting in low underwater oil contact angle (OCA) values, indicative of hydrophobicity. After PVA/GA coating, the smoother, hydrophilic surface prevents oil adhesion[39]. The PVA layer bonds strongly with water, repelling oils and leading to high OCA values for chloroform, hexadecane, and soybean oil, confirming enhanced oleophobicity. The more uniform surface further limits oil interaction, preventing penetration or adhesion[21].

The PVDF/GTA membrane, fabricated using GTA as the extruded solvent, exhibited the largest pore size among the tested membranes. Its hierarchical structure and rougher surface significantly improved the effectiveness of the PVA/GA coating. The increased surface roughness provided a larger contact area for the coating, ensuring better adhesion, crosslinking, and distribution[40]. Additionally, the larger pores allowed deeper penetration of the PVA/GA coating, forming a more integrated hydrophilic layer rather than just a surface coating. This enhanced hydrophilicity improved water adsorption and diffusion, contributing to increased water permeance. Furthermore, the rough surface morphology reduced oil adhesion, reinforcing the membrane's oleophobic and self-cleaning properties[41].

The permeance and oil rejection for soybean O/W emulsion before and after PVA/GA coating are shown in Fig. 3a. The uncoated PVDF membrane exhibited the lowest permeance of 1616 LMH/bar, which was similar to its pure water permeance, due to its dense surface. The PVDF/GTA membrane showed a permeance of 2628 LMH/bar, while the PVDF/PC membrane had a permeance of 1936 LMH/bar. After PVA/GA coating, the permeance of the soybean O/W emulsion increased to 2207 LMH/bar for M-PVDF, 2737 LMH/bar for M-PVDF/GTA, and 2609 LMH/bar for M-PVDF/PC.

Before PVA/GA coating, the hollow fiber membranes with nanoscale pores could remove oil droplets larger than the pore size, but their high hydrophobicity led to incomplete removal, with some oil droplets adhering to the surface. As a result, the oil rejection efficiencies were 78.9% for PVDF, 86.5% for PVDF/GTA, and 87.0% for PVDF/PC, which were insufficient for effective oil-water separation.

After PVA/GA coating, the oil rejection significantly improved, with values of 98.3% for M-PVDF, 99.8% for M-PVDF/GTA, and 99.1% for M-PVDF/PC. These results demonstrate the membranes' suitability for oil-water separation applications, such as industrial wastewater treatment, marine oil spill cleanup, and refining processes, where efficiencies above 95% are required.

Figure 3b illustrates the performance of the M-PVDF/GTA membrane, which showed the best results. The O/W permeance and oil rejection for soybean oil were 2737 LMH/bar and 99.8%, respectively. For chloroform, hexane, and hexadecane oils, the O/W permeance and rejection values were 2489 LMH/bar and 99.1%, 2537 LMH/bar and 99.5%, and 2259 LMH/bar and 99.6%, respectively. The M-PVDF/GTA membrane achieved over 99% oil rejection for all tested oils.

The best-performing membrane in this work (M-PVDF/GTA) was compared to other membranes for oil-in-water emulsion separation reported in literature, as shown in Table S5. The M-PVDF/GTA membrane exhibited high emulsion permeance of above 3000 LMH/bar for all emulsions tested in this work, while maintaining oil rejection above 99%, comparable to the other best-performing membranes reported.

Discussion

This study demonstrates the successful fabrication of high-performance hollow fiber membranes for oil-water separation by regulating their porous structure and surface properties. By introducing an extruded solvent during

the thermally induced phase separation process, membrane porosity and pore size were effectively controlled, leading to significant improvements in water permeance. The highest porosity and permeance were achieved with glycerol triacetate (GTA) as the extruded solvent. Further modification with a polyvinyl alcohol coating resulted in a superhydrophilic and superoleophobic membrane composite, achieving complete water absorption (0° contact angle) while preventing oil droplet adhesion.

The self-cleaning ability of PVDF/GTA membranes was evaluated using Oil Red O dye in soybean oil and chloroform. Uncoated membranes exhibited strong oil adhesion, while PVA-coated M-PVDF/GTA membranes repelled oil, enabling easy removal. Anti-fouling tests showed that coated membranes retained significantly higher permeability and flux recovery ratios (FRR) compared to uncoated ones. PVA/GA-coated membranes demonstrated over 90% FRR for various oil emulsions, with the M-PVDF/GTA membrane maintaining over 82% of its initial flux after three days. Hydrophilic PVA/GA coating improved water spreading, reduced oil adhesion, and enhanced oleophobicity. The rougher PVDF/GTA membrane surface allowed better PVA/GA coating adhesion, improving hydrophilicity, water permeance, and fouling resistance. These findings confirm that PVA/GA-modified membranes exhibit excellent self-cleaning, anti-fouling, and oil-repellent properties, making them highly suitable for prolonged oil-water separation applications. The coated membranes demonstrated excellent antifouling performance, with a flux recovery ratio (FRR) exceeding 90%, compared to lower than 30% for uncoated membranes.

The permeance and oil rejection of soybean oil-in-water emulsions were assessed before and after PVA/GA coating. Uncoated membranes exhibited lower permeance due to their hydrophobic nature, with PVDF, PVDF/GTA, and PVDF/PC membranes showing permeance values of 1616, 2628, and 1936 LMH/bar, respectively. After coating, permeance improved to 2207, 2737, and 2609 LMH/bar for M-PVDF, M-PVDF/GTA, and M-PVDF/PC, respectively. Oil rejection was initially low (78.9% for PVDF, 86.5% for PVDF/GTA, and 87.0% for PVDF/PC) due to surface oil adhesion. After PVA/GA coating, rejection rates increased significantly to 98.3%, 99.8%, and 99.1%, demonstrating effective oil-water separation. The M-PVDF/GTA membrane showed the best performance, achieving over 99% rejection for various oils, including chloroform, hexane, and hexadecane. These findings highlight the potential of fabricating superhydrophilic and superoleophobic membranes through simple structural regulation, offering a scalable and effective solution for oil-water separation applications.

Methods

Materials

Poly(vinylidene fluoride) (PVDF) (type 6020, Mw: 670–700 kDa) was kindly provided by Solvay Soiexis K.K. (Tokyo, Japan) and used as a membrane material. Glycerol triacetate (GTA), propylene carbonate (PC), isopropanol (IPA), and ethanol were purchased from Wako Pure Chemical Industries (Osaka, Japan). Polyvinyl alcohol (PVA, Mw: 89,000–98,000, 99+ % hydrolyzed), glutaraldehyde (GA), acetone, hydrochloric acid (HCl), chloroform, soybean oil, hexane, hexadecane, toluene, petroleum ether, sodium dodecyl sulfate (SDS), Tween 80, and Oil Red O were purchased from Wako Pure Chemical Industries (Osaka, Japan). Crude oil was purchased from Sigma Aldrich (Japan). Galwick was supplied by Porous Material, Inc. (Ithaca, USA) and used for the measurement of pore size. Pure water was produced by a Millipore Milli-Q unit. All chemicals used in this work were used as received. In this work, the chemical (GTA) that dissolved PVDF is referred to as the "diluent," while the chemical (GTA, PC) that extruded at the outer surface of the PVDF dope solution is referred to as the "solvent."

Hollow fiber membrane fabrication

PVDF hollow fiber membranes were prepared by the TIPS process using a twin-screw extruder (TW05, ULTNano, Japan) and triple-orifice spinneret, as shown in Figure S4[42]. First, GTA was melted at 190 °C and then fed into the extruder at 190 °C and a flow rate of 5.95 g/min, which was controlled by a metering pump (5GU30KB, Oriental Motor Co., Ltd., Japan). At the same time, PVDF was fed into the extruder at a constant rate of 2.55 g/min for dissolution. After releasing the air bubbles in the heated zones of the extruder barrel, the homogenous polymer solution was transported to a metering pump (Kawasaki Heavy Industry LTD, Japan) at a pressure of 1.5 MPa. The metering pump forced the PVDF solution through the middle channel of a triple-orifice spinneret, which was purchased from Kasen Nozzle Mfg. Co., Ltd., at a constant rate of 8.5 g/min. The details of the triple-orifice spinneret are shown in Figure S4. In the inner channel of the spinneret, GTA was used as a bore liquid and was extruded by a gear pump (5GU30KB, Oriental Motor Co., Ltd., Japan) to form the lumen of the hollow fibers. An extruded solvent flowed simultaneously through the outermost channel of the triple orifice spinneret at a constant rate of 2 g/min, driven by a peristaltic pump (Chuo Rika LTD, Japan). This was used to tailor the surface and sublayer structures of the hollow fiber membranes. After passing through an air gap of 10 cm, the extruded hollow fibers were immersed in a water quenching bath to induce phase separation and solidification and then wound on a take-up winder. Finally, GTA in the membrane was extracted by immersion in ethanol at room temperature for at least one week and ethanol changed every day to ensure the total removal of GTA from the membrane. The prepared membranes were stored in Pure water for subsequent characterization and tests. The outer diameters of the prepared membranes were approximately 900 nm, and the inner diameters were approximately 600 nm. The preparation conditions and parameters of the hollow fiber membranes are listed in Table S6. The GTA used in the preparation of the polymer solutions is referred to as the "diluent" and the solvent extruded to control the membrane structure is termed the "extruded solvent". The normal PVDF membrane was a PVDF membrane prepared without extruded solvent at the outer surface of the polymer solution. The solvents were selected to control the outer surfaces of the prepared membranes based on their solubility parameter and are listed in Table S6.

Modification of PVDF hollow fiber membrane via PVA dip coating

The PVDF hollow fiber membranes were modified to increase its hydrophilicity via PVA dip coating and crosslinking methods, as shown in Figure S15[27]. 1 wt% of PVA dipping solution was prepared in water at 95 °C with constant stirring for 6 h, and the solution was kept in a dry oven at 60 °C. Prior to PVA dip coating, the nanofiber mats were pre-wetted by soaking in IPA for 1 min, then rinsed with deionized (DI) water several times to remove the residual IPA. To remove the residual water on the hollow fibers, the PVDF hollow fibers were sandwiched in paper towels. The hollow fibers were then soaked in PVA solution at 60 °C for 1 h. An air gun was used to remove the excess PVA solution. Then, the samples were dried in the oven at 100 °C for 10 min. The PVA coated on the PVDF hollow fibers was subsequently crosslinked by soaking the membranes in a solution containing 50 mM GA and 20 mM HCl in acetone/DI water (5:5 volume ratio) for 1 h at room temperature. After the cross-linking reaction, the samples were cured at 100 °C for 10 min to enhance the cross-linking reaction. The modified hollow fibers were then stored in DI water prior to use. Table S8 lists the membranes prepared in this work.

Characterization of hollow fiber membrane

Membrane morphology observation. A field emission scanning electronic microscope (SEM, AIS23000C, Seron Tech Co., Korea) was used to observe the morphology of the PVDF membranes. The cross-sectional samples were fractured in liquid nitrogen prior to imaging. Both the surface and cross-sectional samples were freeze-dried in a freeze dryer (FDU-1200 EYELA; Tokyo Rikakikai Co., Ltd, Tokyo, Japan) overnight and then sputter-coated with a thin Au layer of about 5 nm thickness using an ion sputter coater (G20, GSEM Co., Ltd, Korea). SEM images of all membranes with different magnifications were obtained at an accelerating voltage of 20 kV.

Chemical composition analysis. The chemical structure of the prepared PVDF membranes entrapped with surfactants was analyzed using a Fourier transform infrared spectroscopy (FTIR-ATR) spectrometer (ALPHA FTIR spectrometer, Bruker Optics) with the wavenumber between 450 and 1500 cm^{-1} and results were compared with that of the control PVDF membrane. X-ray photoelectron spectroscopy (XPS; JPS-9010 MC; JEOL Ltd. Tokyo, Japan) with an Al Kα radiation source (1486.6 eV) was used to analyze chemical compositions of the membrane surfaces.

Pore size measurement. A liquid–liquid porometer (LLP-1100A, Porous Material Inc., Ithaca, USA) was used to measure the mean pore size of the membranes. Before testing, all hollow fiber membranes were loaded in aluminum tubes in the form of a U-shape using a two-component resin. IPA was used to saturate the pores in the membranes. Galwick, another liquid immiscible with IPA, was utilized to displace the IPA from the pores by applying a differential pressure. A balance detected the presence of pores by sensing the increase in the flow rate at a given applied differential pressure. The differential pressures and flow rates through the wet and dry membranes were measured and used to evaluate the mean pore diameter. The simplified Cantor equation (Eq. (1)) was used to calculate the pore diameters, D (m), because the contact angle of IPA on the membrane was close to zero.

$$D = \frac{4\gamma}{P} \tag{1}$$

where, P is the applied pressure (Pa) and γ is the interfacial tension of IPA (N/m).

Surface charge analysis of membranes. The surface zeta potentials of the membrane samples were investigated by electrokinetic analyzer (SurPASS™ 3; Anton Paar; Graz, Austria) using a 75 ppm KCl electrolyte solution.

Mechanical strength measurement. The mechanical strength of PVDF membranes was measured by a precision tensile testing apparatus (AGS-J, Shimadzu Co., Japan). All samples were vertically fixed between two pairs of tweezers with a length of 20 mm and then stretched at a constant rate of 20 mm/min until broken.

Hydrophilicity and underwater oleophobicity evaluation. A contact angle goniometer (Drop Master, Kyowa Interface Science Co., Japan) was used to measure the water contact angle for the outer surface of the dry membrane. A small droplet of water with the volume of 0.2 μL was dropped onto the membrane surface in air, and then the water contact angle of the PVDF membrane was measured by using images taken by the camera. Each membrane was analyzed at least three times by using different pieces of membrane. In this study, the WCA of the prepared membranes were measured just after dropping the water droplet and 5 min after dropping the water on the membrane surface.

Pure water permeability evaluation. The filtration performance measurements for wet and dried hollow fiber membranes were carried out using a laboratory-scale apparatus in which the water was flown from the outside to the inside under the pressure of 0.05 MPa. The measurement was done after keeping the membrane under the pressure of 0.05 MPa for 30 min for compaction and reaching stable pure water permeability. The membrane pure water permeability (PWP, $L/m^2 \cdot h \cdot bar$) was estimated by the following equation.

$$PWP = \frac{V}{A \times t \times P} \tag{2}$$

where V (L) is the volume of water collected in the running time of t (h), A (m^2) is the effective surface area for testing and P is transmembrane pressure. Five pieces of the membrane were measured in parallel for each sample.

Fouling analysis. The fouling propensity of the membranes were assessed by filtration experiments using different oil-in-water (O/W) emulsions. The oil droplet size distributions in O/W emulsions were measured by dynamic light scattering (DLS; ELSZ-1000 ZA; Otsuka Electronics Co. Ltd. Osaka, Japan). Optical microscope (BX50, Olympus, Tokyo, Japan) was used to observe the distributed oil droplets in water for the feed emulsions and permeated water.

The rejection ratio (RR) of different O/W emulsions was estimated by examining the oil contents before and after membrane separation by using a total organic carbon (TOC) analyzer (TOC-VCSH, Shimadzu, Japan). On the other hand, the rejection ratios of different W/O emulsions were estimated by measuring the water contents using a Karl Fischer titrator (MKH-700, KEM, Kyoto, Japan). In both cases, the rejection (R) values were calculated according to Eq. (3).

$$R = \left(1 - \frac{C_2}{C_1}\right) \times 100\,\% \tag{3}$$

where C_1 and C_2 are the oil content (in O/W emulsions) before and after membrane filtration, respectively. The antifouling test consists of three filtration cycles, where each cycle starts with oily emulsions filtration for 1 h, and the initial flux was recorded as *J1*. After each cycle, the membrane was washed by water to remove the surface oil, and the recovered oily emulsion flux was recorded as J_2. The fouling-resistant/fouling-releasing property of the membrane against oily emulsion was evaluated by calculating the flux recovery ratio (FRR), using Eq. (4):

$$FRR = \frac{J_2}{J_1} X100\,\% \tag{4}$$

Data Availability

No datasets were generated or analysed during the current study.

Received: 10 February 2025; Accepted: 14 April 2025;
Published online: 10 May 2025

References

1. Gonzales, R. R. et al. Facile development of comprehensively fouling-resistant reduced polyketone-based thin film composite forward osmosis membrane for treatment of oily wastewater. *J. Membr. Sci.* **626**, 119185 (2021).
2. Hu, M. et al. One-Step Phase Separation and Mineralization Fabrication of Membranes for Oily Wastewater Treatment. *ACS Appl. Mater. Interfaces* **16**, 38723–38732 (2024).
3. Huang, J., Ran, X., Sun, L., Bi, H. & Wu, X. Recent advances in membrane technologies applied in oil–water separation. *Discov. Nano* **19**, 66 (2024).
4. Mehri, M., Fallah, N. & Nasernejad, B. Mechanisms of heavy metal and oil removal from synthetic saline oilfield produced water by electrocoagulation. *npj Clean Water* **4**, 45 (2021).
5. Ye, Q. et al. Metal-organic framework modified hydrophilic polyvinylidene fluoride porous membrane for efficient degerming selective oil/water emulsion separation. *npj Clean Water* **5**, 23 (2022).
6. Wang, X. et al. Preparation of superhydrophilic/underwater superoleophobic membranes for separating oil-in-water emulsion: mechanism, progress, and perspective. *J. Coat. Technol. Res.* **18**, 285–310 (2021).
7. Zhang, L., Lin, Y., Cheng, L., Yang, Z. & Matsuyama, H. A comprehensively fouling- and solvent-resistant aliphatic polyketone membrane for high-flux filtration of difficult oil-in-water micro- and nanoemulsions. *J. Membr. Sci.* **582**, 48–58 (2019).

8. Zhang, L. et al. In situ engineering of an ultrathin polyamphoteric layer on polyketone-based thin film composite forward osmosis membrane for comprehensive anti-fouling performance. *Sep. Purif. Technol.* **272**, 118922 (2021).
9. Zhang, Y., Yang, J., Zhao, Y., Wang, Z. & Lai, G. S. Anti-fouling ternary zwitterionic coating membrane with strong surface hydration and salt resistant for efficient long-term emulsion separation in high salinity marine environment. *J. Membr. Sci.* **710**, 123167 (2024).
10. Baig, N., Abdulazeez, I., Khan, N. A. & Hanif, M. B. Experimental and theoretical assessment of bioinspired next-generation intercalated graphene oxide-based ceramic membranes for oil-in-water emulsion separation. *npj Clean Water* **7**, 82 (2024).
11. Tian, X. et al. Nacre-inspired graphene oxide/polyethyleneimine-based ultra-thin heterogeneous superwetting membrane for highly stable separation of oil-in-water emulsions. *Sep. Purif. Technol.* **356**, 129991 (2025).
12. Baig, U., Waheed, A., Yogarathinam, L. T. & Aljundi, I. H. Tailored alumina nanocomposite membranes featuring MIL-125-NH2 metal-organic frameworks for oily wastewater treatment. *npj Clean Water* **7**, 26 (2024).
13. Hong, L. et al. A superhydrophobic PVDF-based membrane containing Metal-organic framework for efficient Oil-water separation. *Mater. Sci. Eng.: B* **310**, 117684 (2024).
14. Gonzales, R. R. et al. Enhanced water permeability and osmotic power generation with sulfonate-functionalized porous polymer-incorporated thin film nanocomposite membranes. *Desalination* **496**, 114756 (2020).
15. Yang, W. et al. Covalent organic frameworks-coated silk membrane for durably efficient oil/water separation. *React. Funct. Polym.* **198**, 105885 (2024).
16. Zeng, Q. et al. Exceptional self-cleaning MXene-based membrane for highly efficient oil/water separation. *J. Membr. Sci.* **700**, 122691 (2024).
17. Li, Y. et al. Unique dual superlyophobic covalent organic frameworks (COF-TpBD) intercalated MXene composite membrane for efficient oil-water separation. *J. Membr. Sci.* **717**, 123579 (2025).
18. Hu, X. et al. Novel conductive Janus membranes with water diode effect assisted by an electrostatic field for efficient mass transfer and oil-water separation. *J. Membr. Sci.* **708**, 123037 (2024).
19. Wang, N., Zhai, Y., Yang, Y., Yang, X. & Zhu, Z. Electrostatic assembly of superwetting porous nanofibrous membrane toward oil-in-water microemulsion separation. *Chem. Eng. J.* **354**, 463–472 (2018).
20. Xu, T. et al. A slippery hydrogel coating with durable oil-repellent property and self-regeneration capacity. *Sci. China Technol. Sci.* **65**, 1819–1827 (2022).
21. Yan, L. et al. Nanocomposite hydrogel engineered hierarchical membranes for efficient oil/water separation and heavy metal removal. *J. Membr. Sci.* **668**, 121243 (2023).
22. Gu, Y. et al. Poly (vinyl alcohol) modification of poly (vinylidene fluoride) microfiltration membranes for oil/water emulsion separation via an unconventional radiation method. *J. Membr. Sci.* **619**, 118792 (2021).
23. Sharma, G. et al. Applications of nanocomposite hydrogels for biomedical engineering and environmental protection. *Environ. Chem. Lett.* **16**, 113–146 (2018).
24. Gonzales, R. R. et al. Hydrogel membrane composite reduces fouling and retains ammonium efficiently. *Environ. Chem. Lett.* **22**, 1615–1621 (2024).
25. Fang, C. et al. Hollow fiber membranes with hierarchical spherulite surface structure developed by thermally induced phase separation using triple-orifice spinneret for membrane distillation. *J. Membr. Sci.* **618**, 118586 (2021).
26. Zhang, P. et al. Wetting-and scaling-resistant superhydrophobic hollow fiber membrane with hierarchical surface structure for membrane distillation. *J. Membr. Sci.* **693**, 122338 (2024).
27. Park, M. J., Gonzales, R. R., Abdel-Wahab, A., Phuntsho, S. & Shon, H. K. Hydrophilic polyvinyl alcohol coating on hydrophobic electrospun nanofiber membrane for high performance thin film composite forward osmosis membrane. *Desalination* **426**, 50–59 (2018).
28. Zhang, P. et al. Hierarchically Structured Porous Polyamide-Imide Membrane for Switchable Emulsion Separation. *Adv. Mater.* **n/a**, 2501092 (2025).
29. Fang, C. et al. Tailoring the surface pore size of hollow fiber membranes in the TIPS process. *J. Mater. Chem. A* **6**, 535–547 (2018).
30. Wang, Z., Sun, L., Wang, Q., Li, B. & Wang, S. A novel approach to fabricate interconnected sponge-like and highly permeable polyvinylidene fluoride hollow fiber membranes for direct contact membrane distillation. *Eur. Polym. J.* **60**, 262–272 (2014).
31. Yang, J. et al. Formation of a bicontinuous structure membrane of polyvinylidene fluoride in diphenyl ketone diluent via thermally induced phase separation. *J. Appl. Polym. Sci.* **110**, 341–347 (2008).
32. Lin, Y. et al. Formation of a bicontinuous structure membrane of polyvinylidene fluoride in diphenyl carbonate diluent via thermally induced phase separation. *J. Appl. Polym. Sci.* **114**, 1523–1528 (2009).
33. Kim, S. S. & Lloyd, D. R. Microporous membrane formation via thermally-induced phase separation. III. Effect of thermodynamic interactions on the structure of isotactic polypropylene membranes. *J. Membr. Sci.* **64**, 13–29 (1991).
34. Umakoshi, K. et al. Effect of polymer-solvent compatibility on polyamide hollow fiber membranes prepared via thermally induced phase separation. *Colloids Surf. A: Physicochem. Eng. Asp.* **642**, 128704 (2022).
35. Xiang, S. et al. Fabrication of high-permeance polyketone (PK) hollow fiber membrane using triple-orifice spinneret via the thermally induced phase separation. *J. Membr. Sci.* **695**, 122511 (2024).
36. Zhang, P. et al. Understanding the multiple functions of styrene-co-maleic anhydride in fabricating polyvinylidene fluoride hollow fiber membrane via coupled phase inversion process and its effect on surface infiltration behavior and membrane permeability. *J. Membr. Sci.* **590**, 117269 (2019).
37. Li, X., Chen, Y., Hu, X., Zhang, Y. & Hu, L. Desalination of dye solution utilizing PVA/PVDF hollow fiber composite membrane modified with TiO2 nanoparticles. *J. Membr. Sci.* **471**, 118–129 (2014).
38. Wang, K. et al. Chemically Crosslinked Hydrogel Film Leads to Integrated Flexible Supercapacitors with Superior Performance. *Adv. Mater.* **27**, 7451–7457 (2015).
39. Wang, K. et al. Hydrophilic surface coating on hydrophobic PTFE membrane for robust anti-oil-fouling membrane distillation. *Appl. Surf. Sci.* **450**, 57–65 (2018).
40. Croll, S. G. Surface roughness profile and its effect on coating adhesion and corrosion protection: A review. *Prog. Org. Coat.* **148**, 105847 (2020).
41. Hegab, H. M. et al. 3D hierarchical aquaporin-like nanoporous graphene membrane with engineered tripartite nanochannels for efficient oil/water separation. *npj Clean Water* **7**, 10 (2024).
42. Zhang, P. et al. Effect of polymer molecular weight on structure and performance of PVDF hollow fiber membranes prepared via TIPS process with co-extrusion of solvent using triple orifice spinneret. *J. Membr. Sci.* **620**, 118854 (2021).

Acknowledgements

This study was supported by Korea Institute for Advancement of Technology (KIAT) grant funded by the Korea Government (MOTIE) (P0017310, Human Resource Development Program for Industrial Innovation (global)) and was partially supported by International Membrane Hub and Kobe University Strategic International Collaborative Research Grant (Type B Fostering Joint Research). This research was also supported by Basic Science Research Program through the National

Research Foundation of Korea (NRF) funded by the Ministry of Education (RS-2020-NR049575).

Author contributions

All authors contributed to study conception and design; Hyun Woong Kwon, Ralph Rolly Gonzales, Pengfei Zhang, Bowen Li, Jun Ho Park, Tae Kyung Lee: Material preparation, data collection, analysis; Hyun Woong Kwon, Ralph Rolly Gonzales, Kwang Seop Im: writing; Ralph Rolly Gonzales, Hideto Matsuyama, Sang Yong Nam: review and editing; Sang Yong Nam, Hideto Matsuyama: supervision and fund acquisition. All authors read and approved the final manuscript.

Competing interests

The authors declare no competing interests.

Additional information

Supplementary information The online version contains supplementary material available at https://doi.org/10.1038/s41545-025-00468-0.

Correspondence and requests for materials should be addressed to Hideto Matsuyama or Sang Yong Nam.

Reprints and permissions information is available at http://www.nature.com/reprints

Publisher's note Springer Nature remains neutral with regard to jurisdictional claims in published maps and institutional affiliations.

Open Access This article is licensed under a Creative Commons Attribution-NonCommercial-NoDerivatives 4.0 International License, which permits any non-commercial use, sharing, distribution and reproduction in any medium or format, as long as you give appropriate credit to the original author(s) and the source, provide a link to the Creative Commons licence, and indicate if you modified the licensed material. You do not have permission under this licence to share adapted material derived from this article or parts of it. The images or other third party material in this article are included in the article's Creative Commons licence, unless indicated otherwise in a credit line to the material. If material is not included in the article's Creative Commons licence and your intended use is not permitted by statutory regulation or exceeds the permitted use, you will need to obtain permission directly from the copyright holder. To view a copy of this licence, visit http://creativecommons.org/licenses/by-nc-nd/4.0/.

© The Author(s) 2025